IDENTIFICATION OF GROUNDWATER BASIN SHAPE AND BOUNDARY USING HYDRAULIC TOMOGRAPHY

by

Kwankwai Daranond

A Thesis Submitted to the Faculty of the

DEPARTMENT OF HYDROLOGY AND ATMOSPHERIC SCIENCES

In Partial Fulfillment of the Requirements

For the Degree of

MASTER OF SCIENCE
WITH A MAJOR IN HYDROLOGY

In the Graduate College

THE UNIVERSITY OF ARIZONA

2019

THE UNIVERSITY OF ARIZONA
GRADUATE COLLEGE

As members of the Master's Committee, we certify that we have read the thesis prepared by Kwankwai Daranond, titled *Identification of groundwater basin shape and boundary using Hydraulic Tomography* and recommend that it be accepted as fulfilling the dissertation requirement for the Master's Degree.

Tian-Chyi Jim Yeh Date: 11/22/19

Paul A. Ferre Date: 11/22/19

Thomas Meixner Date: 11/22/19

Final approval and acceptance of this thesis is contingent upon the candidate's submission of the final copies of the thesis to the Graduate College.

I hereby certify that I have read this thesis prepared under my direction and recommend that it be accepted as fulfilling the Master's requirement.

Tian-Chyi Jim Yeh Date: 11/22/19
Master's Thesis Committee Chair
Department of Hydrology and Atmospheric Sciences

ACKNOWLEDGEMENTS

First, I would like to thank Prof. Jim Yeh, who always has recommendations, and challenges me with questions about my research. I also would like to thank committee members for pointing out some details which are important to be recognized. Many thanks to every student in our research group for helping me out of problems on my project along these years. In addition, I would like to thank Dr. Donald Slack for giving me chances to have presentations of my research at your department as well as in Sinaloa, Mexico.

Many thanks to the Royal Thai Government for giving me an opportunity to study abroad and for all supports while I was studying at the University of Arizona.

Many thanks to my family and friends who always brighten my world.

Table of Contents

Section *Page*

List of Tables (Appendix A)

List of Figures (Appendix B)

ABSTRACT

Shapes and boundary types of a groundwater basin play important roles in the analysis of groundwater management and contaminant migration. Hydraulic tomography (HT) is a recently developed new approach for high-resolution characterization of aquifers. HT is not only an inverse methodology but also a logic data collection approach for non-redundant hydraulic information to provide high-resolution characterizations of aquifers. In this study, HT was applied to synthetic 2-D aquifers to investigate its feasibility to map the irregular shapes and types of the aquifer boundaries. We first used the forward model of VSAFT2 to simulate hydraulic responses of aquifers due to pumping tests under combinations of irregular geometries and different boundary conditions, e.g., constant head, and no-flow boundaries. Then, we used SimSLE (Simultaneous Successive Linear Estimator) inverse model in VSAFT2 to estimate the spatial distribution of hydraulic properties within rectangular-shaped domains with constant head boundaries. The simulations were conducted in both steady and transient states using a similar monitoring network to assess the ability of HT for detecting types and shapes of the boundary. Furthermore, the improvement of the estimation with prior information of transmissivity and storage coefficient was investigated. These cases were conducted using Monte Carlo simulations to ensure statistical meaningful conclusions.

INTRODUCTION

To study the availability of groundwater or migration of contaminants in an aquifer, the aquifer characteristics have to be determined. Generally, the conventional pumping test analyses, for instance, Theis (Theis, 1935) and Cooper-Jacob (Cooper and Jacob, 1946), have been widely adopted to estimate the aquifer characteristics. However, these methods do not provide sufficient information for a high-resolution prediction. In order to increase the accuracy of the prediction, a large amount of aquifer information is required.

In the past decades, the method of Hydraulic Tomography (HT) (Yeh and Liu, 2000) has been developed. In this method, series of pumping tests are conducted by relocating the location of the pumping well and treating the rest of the existing wells within the same well field as the observation wells (Yeh and Lee, 2007). Thus, HT allows us to gather non-redundant information of the aquifer from a limited number of wells. The collection of non-redundant information can improve the estimation of heterogeneity (Wen et al., 2019). This improvement has also been validated by many experiments of HT in synthetic aquifers, laboratory sandboxes, and field operations (e.g., Yeh and Liu, 2000; Liu et al., 2002; Zhu and Yeh, 2005; Liu et al., 2007; Straface et al., 2007; Ni et al., 2009; Yin and Illman, 2009; Bohling and Butler, 2010; Wen et al., 2010; Cardiff and Barrash, 2011; Huang et al., 2011; Berg and Illman, 2012; Cardiff et al., 2012; Illman et al., 2015; Tso et al., 2016; Zha et al., 2016).

While HT is useful, many efforts to improve the estimation of hydraulic properties using HT has been proposed. For instance, the geological knowledge is employed for initial information in order to examine whether it can improve the heterogeneity estimation as discussed by Zhao et al. (2016). Cardiff and Barrash (2011) also combine the knowledge of geological data with HT

and investigate the effect of S on the heterogeneity characterization. However, a small number of studies have inspected the role of S on the aquifer characteristics using HT.

The boundary condition in the previous experiments in synthetic aquifers or laboratory sandboxes is generally known. The known boundary condition likely minimizes the uncertainty in the aquifer estimation. On the other hand, the field HT experiment involves uncertainty in the boundary. To reduce the effects of the uncertain boundary condition, a large domain compared to the size of the well-field was often created (Straface et al., 2007; Lu et al., 2012; Sun et al.,2013). Although Sun et al. (2013) also studied the effect of the incorrect boundary condition, they only considered the rectangular domain. The effects of irregular boundary shape on the estimation has not been fully investigated.

In this study, we employ HT in a synthetic heterogeneous aquifer to investigate its ability to delineate the geometry of boundary and associated boundary conditions. We also investigate the effect of this incorrectly assigned boundary condition on the parameter estimation in the basin area. Moreover, the effects of prior information of storage coefficient on estimated T and S are also examined.

METHODOLOGY

1. Governing Flow Equation

A two-dimensional, horizontal groundwater flow model in saturated, heterogeneous media is created and simulated by using VSAFT2 (Variably Saturated Flow and Transport in two dimensions) (Yeh et al., 1993). The flow of groundwater is described by the following partial differential equation,

$$\nabla \cdot [T(\boldsymbol{x})\nabla H] + Q(\boldsymbol{x}_p) = S(\boldsymbol{x})\frac{\partial H}{\partial t} \quad (1)$$

which is dependent on the boundary and initial condition,

$$H|_{\Gamma 1} = H_1,\ [T(\boldsymbol{x})\nabla H] \cdot \boldsymbol{n}|_{\Gamma 2} = q \quad \text{and} \quad H|_{t=0} = H_0 \quad (2)$$

where T(**x**) is the transmissivity [L^2/T], $\overline{H}$ is the total head [L], Q($\mathbf{x}_p$) is the pumping rate [L^3/T] at location x_p, S(**x**) is the storage coefficient [-], H_1 is the prescribed total head at Dirichlet boundary Γ_1, q is the prescribed flux at the Neumann boundary Γ_2, $\boldsymbol{n}$ is a unit vector normal to the boundary, and H_0 is the total head before applying any stress to the aquifer. The term on the right-hand side of equation 1 will be zero if the simulation is in a steady-state representing no change of water in storage through time.

2. Model Setup

In order to create a synthetic heterogeneous aquifer, we adopt the stochastic concept (Yeh, 1992; Yeh et al., 2015), which treats T and S as random variables. This heterogeneous medium is described by defining mean, variance, and correlation scale. With the same description, we could obtain an infinite number of heterogeneity patterns or realizations.

In this study, an aquifer is conceptualized based on a buried-valley aquifer. This type of aquifer consists of many facies of glacial sedimentation, which are heterogeneous (Anderson, 1989). The heterogeneous medium is generated based on the stochastic concept. The aquifer is synthesized within an irregular domain as shown in Figure 1a. Mean InT, variance lnT, mean lnS, variance lnS, and correlation scale in x and y are -1.5, 1.61, -7.5, 1.10, and 50 m, respectively. The left and right boundaries are no-flow boundaries representing impermeable parts of the valley. The top and bottom boundaries are constant head boundaries portraying permeable bodies in the valley.

Nine wells are installed into the synthesized heterogeneous aquifer, displayed as red and black circles in Figure 1. Red circles are the location of wells that are used as both pumping and observation wells. Black circles are locations of observation wells. Five sequential pumping tests are conducted based on the HT survey. The flow fields are simulated by the governing equations and solved by VSAFT2. Each pumping event is performed at each red circle while the rest of the wells are treated as observation wells. Five sets of drawdown data are collected in both steady and transient states.

With the same well-field, many realizations of the heterogeneity based on the aforementioned mean, variance, and correlation scale are generated based on Monte Carlo simulation. The random hydraulic properties fields are used to explore the effect of different heterogeneity patterns contributing to drawdowns. Then, the drawdown data collected from different heterogeneous materials are applied to each case of the inverse simulation, and the estimated T and S will be obtained.

3. Inverse modeling approach

In this process, models with different prior knowledge of basin geometry, boundary condition, and storage coefficient are applied to investigate the effect of this information on the

estimated T and S. The model using correct boundary geometry and boundary condition (Figure 1a) is used to compare its results with models using rectangular boundary and incorrect boundary condition (Figures 1b and 1c). In each following case, average values of T are assigned as initial guesses of the parameter.

Case 1: The correct irregular shape and boundary conditions are applied to the inverse model (Figure 1a). The average T value of the synthetic material inside the basin is set as an initial guess. In this case, we will focus only on the estimated T and S inside the basin, which are not affected by uncertainty in the aquifer shape and boundary condition.

Case 2: The aquifer is bounded by a square boundary covering both permeable and impermeable parts of the synthetic aquifer. In this case, the previously specified impermeable boundaries and materials are replaced by a constant head boundary. One initial guess of T based on the average T of permeable material in the basin is given to the square domain (Figure 1b).

Case 3: The shape of the domain and boundary condition is similar to the description in Case 2. In addition to that, geology information is assumed to be known but not exact locations to the true synthetic aquifer boundary. The impermeable material is delineated at areas close to the corners of the domain as shown as the black areas in Figure 1c. Initial guesses of this case are separated into two zones based on average T values of the material in the basin and impermeable material outside the basin.

Models in these three cases are simulated in both steady and transient states. Since S influences the flow to a well at the early time of pumping test (Sun et al. 2013; Mao et al., 2013), we also consider the role of S on the estimated T in transient state. Subcases are denoted with letters A, B, and C.

Condition A: Steady-state.

Condition B: Transient state with an initial guess of fully described S distribution.

Condition C: Transient state with an initial guess of average S value.

In Condition A and B, only T is estimated due to no role of S in a steady-state and no uncertainty of S in Condition B. On the other hand, both T and S are estimated in Condition C when initial guesses of S are expressed by average values.

Then, the HT observed drawdown data from the synthetic aquifer are applied to the models in each case. Inverse simulations of every case are conducted by using a Simultaneous Successive Linear Estimator or SimSLE (Xiang et al.,2009) to estimate hydraulic properties. Collected drawdown data from every pumping test events are simultaneously employed to estimate T and S. The reiteration is terminated based on the termination criteria of differences in variance and head of the consecutive iteration. The simulation will stop reiterating if these criteria were satisfied.

4. Performance Metrics

The regression metricses are used to evaluate the performance of the inverse simulations. In this study, R^2, L_1, L_2, slope, and intercept from the regression analysis are obtained from the relationship between true and estimated hydraulic properties. Metricses can be calculated by the following equations,

$$R^2 = \left[\frac{N(\sum x_i\hat{x}_i)-(\sum x_i)(\sum \hat{x}_i)}{\sqrt{[N\sum x_i^2-(\sum x_i)^2][N\sum \hat{x}_i^2-(\sum \hat{x}_i)^2]}}\right]^2 \quad (3)$$

$$L_1 = \frac{1}{N}\sum_{i=1}^{N}|x_i - \hat{x}_i| \quad (4)$$

$$L_2 = \frac{1}{N}\sum_{i=1}^{N}(x_i - \hat{x}_i)^2 \quad (5)$$

where N is the total number of elements, i is the element number, x_i is the true value of T or S at the element i th, and $\hat{x}_i$ is the estimated value of T or S at the element i th. Slope and intercept can be found from a linear equation of a regression line.

General interpretations for these metricses are that the higher R^2 indicates the better fitting of the estimates to the reference values. The lower L_1 and L_2 show the less deviation of the estimates from the true values. Slope and intercept should be interpreted together as the slope closes to 1 and the intercept approaches to 0 are the better result.

RESULTS

In this section, the results of the T and S estimation from the simulation of one realization are plotted as examples on a contour, histogram, and scatter plot. The contour plot displays the spatial distribution of the estimated parameters from each case. The histogram plot is used to inspect the range of estimated values of elements inside and outside the basin area compared to the range of the true distribution. The scatter plot is adopted to investigate the relationship between the true and estimated values, including calculating the performance metricses of each case. Then, the mean and standard deviation of performance metricses are calculated over ten realizations and displayed on the bar plot.

The true distribution of T and S of the synthetic aquifer are depicted in Figure 2a and Figure 3a, respectively. With drawdown data from HT survey, the estimates from perfect knowledge of boundary in Case 1 (Figures 2b, 2e, 2h and Figures 3b) can capture the major trends of the heterogeneous T and S. In Case 2 and Case 3 (Figures 2c, 2f, 2i, 2d, 2g, 2j and Figures 3c, 3d), the estimated T and S can display the trend of the heterogeneity in the basin area as well, but anomalies of lower T and S are revealed at the areas close to the incorrectly assigned boundary. As zones of impermeable material are already delineated in Case 3, the estimates at the areas outside the basin can yield lower values than the estimates in Case 2.

To quantify estimated T and S at the region inside and outside the basin, the histogram plot is used to present the distribution of the estimates in these two areas. The reference T and S of the material outside the basin are defined to be 0.001 m^2/day and 1 x 10^{-5} [-], respectively. Only the estimated T and S in Case 2 and Case 3 at the elements outside the true domain (Figure 4 and Figure 5) are plotted on the histogram due to their extended boundary beyond the true boundary. The vertical black dashed lines are the reference value of T and S. As initial guesses of T in Case

2 are assigned to be 0.5 m^2/day to the entire domain, the estimated T tends to distribute in the region where has values higher than 0.001 m^2/day (Figure 4a). The mean values of the estimated T outside the true domain in Case 2A, 2B, and 2C are 0.0457, 0.0343, and 0.0403, respectively. On the contrary, initial guesses of permeable and impermeable zones in Case 3 can yield more distribution of estimated T in the lower-value region (Figure 4b). Mean values of estimated T outside the true boundary in Case 3A, 3B, and 3C are 0.000839, 0.000763, and 0.001093, respectively.

Figure 5 shows the distribution of estimated S outside the true geometry. The distribution of the estimated S at the elements outside the basin is similar to the estimated T in Figure 4. The model with one zone initial guess in Case 2C yields the estimated S distributing in the region where the values are higher than $1x10^{-5}$ (Figure 5a). With two zones initial guesses (Case 3C), the estimated S can yield more distribution in the region where S is lower than $1x10^{-5}$ (Figure 4b) and obtain a smaller mean than which in Case 2C.

The distributions of estimated T inside the true geometry are displayed in Figure 6. Histograms of subcases A, B, and C are overlaid with the true distribution (black solid line). The geometric mean of T of the synthetic aquifer is 0.2236 m^2/day. In this realization, the inverse simulation of Case 1B produces the closest mean to the true mean with a value of 0.2248 m^2/day. The most different is the mean T of Case 2A with the value of 0.1212 m^2/day. In addition, while the distribution in Case 1 is likely similar to the true distribution, the estimated T of Case 2 and Case 3 display their distribution as two peaks. The first peak is in the region lower than the true mean and another is in the region higher than the true mean.

On the contrary, the estimated S inside the true geometry of these three cases (Figure 7) is distributed with one peak which resembles the peak of the true S distribution. The geometric mean

of S of the true material, Case 1C, Case 2C, and Case 3C are $5.77x10^{-4}$, $7.49x10^{-4}$, $6.75x10^{-4}$, and $6.49x10^{-4}$, respectively.

In Figure 8 and Figure 9, the estimates T and S at the elements inside the basin are plotted against the true values of T and S. The yellow color represents areas where have larger data accumulation than areas with darker colors (green and blue). The estimated T from the model with correct boundary geometry and boundary condition in Case 1 (Figures 8a, 8d, 8g) result in higher R^2 and smaller L_1, L_2 of estimated T compared to Case 2 and Case 3. Data points tend to scatter away from the 1:1 line when the model is described with incorrect boundary information.

The scatter plots of S in this realization (Figure 9) tend to spread with the same trend. No significant difference shows among these three cases compared to the scatter plots of T. The values of R^2 of Case 1, Case 2, and Case 3 are 0.5944, 0.5814, and 0.6563, and L_2 are 0.5955, 0.5343, and 0.4387, respectively. From the statistical values, the estimated S from Case 3C in this realization is slightly better than the other cases. However, the rank of the performance metricses of each case is not consistent among different realizations.

Because the inverse problem is not well-defined or under-determined, there are many possible solutions. Results of inverse modeling based on one single realization could be misleading. We, therefore, conducted a Monte Carlo simulation to draw the general conclusion for each case. Specifically, we generated ten realizations of random T and S fields with the given normal distribution with the specified mean, variance, and correlation scales of these parameters. Afterward, using the ten realizations, the inverse modeling for each case was conducted, and the performance metricses of the results of each realization was evaluated. The statistics of the performance metricses were then determined.

Table 1 lists the average and standard deviation of R^2, L_1, L_2, slope, and intercept of the estimated T of each case and subcase of ten realizations and these values are plotted in Figure 10. Based on the statistics of R^2, L_1, and L_2 values, the performance of the estimates varies from one realization to another realization. However, the means of these performance metricses suggest that the simulation of Case 1 results in the highest R^2 and lowest L_1 and L_2, which indicate the smallest discrepancy of the estimates from the true values.

Table 2 displays the average and standard deviation of the performance metricses of estimated S. From the average of ten realizations, the estimated S using the correct boundary model results in the highest R^2 of 0.65 and smallest L_1, L_2 among all of the cases. However, R^2 of the estimated S of these three cases are less different compared to R^2 of the estimated T.

DISCUSSION

1. Identification of basin shape and boundary

In this section, we only consider the estimates of T and S in Case 2 and Case 3, in which the square domains are extended beyond the impermeable material and the boundary condition is incorrect. As a pumping test is being conducted, a drawdown in monitoring wells nearby the no-flow boundary could encounter larger drawdowns than the model without this type of boundary. Thus, the information of this no-flow boundary could be embedded in drawdowns collected from the HT survey. The inverse simulation of HT data with SimSLE can reveal these impermeable zones with lower T (shown in blue zones in Figure 2) close to the left and right boundary. The estimated S in Figure 3 also displays regions of lower S in the areas closed to the incorrectly specified boundaries. In addition, the delineated impermeable material zones in Case 3 can yield the lower estimated T and S at the areas outside the basin more than in Case 2, in which the initial guess is specified with one average value.

To assess the estimates in the areas outside the basin, the distribution of estimated T and S in the impermeable region of Case 2 and Case 3 are plotted on the histogram in Figure 4 and Figure 5. The distributions of estimated T of Case 2 in Figure 4a and estimated S in Figure 5a are larger than the reference value (black dashed line). With one initial guess value based on average T and S of the aquifer, this yields the estimates distributing in the region that has higher T and S than the reference. The two zones of the initial guess of T and S in Case 3 result in the spreading of the estimates into the lower T and S region as displayed in Figure 4b and Figure 5b. The prior assigned smaller number for the impermeable zones improves the estimation of both T and S. However, these two plots of Case 3 still have some estimated T and S distributed in the higher value region due to the inaccurate zone delineation. Some elements outside the basin which falls into the zone

of permeable material will be started with the higher initial guess of T and S. The estimates based on this higher initial guess cannot reach the very low T and S. Therefore, the initial guesses of T and S could influence the estimated T and S.

2. Effects of the incorrect boundary geometries and conditions on the estimation inside the basin

In this part, the estimated T and S from the model with true boundary geometries and conditions (Case1) are considered. This model is used to compare with the estimates inside the basin area from Case 2 and Case 3. With a correctly described boundary, the estimated T of Case 1 (Figures 2a, 2e, 2h) does not display any anomalies of low T zones along the left and right boundary. Similar to the estimated T, the distribution of estimated S in Case 1 (Figure 3b) does not show any particularly low S zones close to the impermeable material.

From the T distribution in Figure 6, Case 2 and 3 tend to have a distribution of the lower T more than in Case 1. The incorrectly described boundary yields the estimation to create the zones of low T along the left and right boundary in order to match the simulated and observed drawdown. Parts of the basin located near the incorrectly assigned boundary would be affected more than the parts located farther away from the boundary. As evidenced in Figure 6, the values of estimated T in Case 2 and Case 3 has humps on the left of its mean value. These anomalies of low T are also shown in Figure 8. Values of the estimated T in Case 2 and Case 3 tend to scatter lower than the 1:1 line and this indicates that the estimated T at some elements is much lower than the true one. However, the distributions of the estimated S which are depicted in Figures 7b and 7c have different characteristics from the estimated T.

The histograms of estimated S show the peak which is similar to the peak of the true S. This distribution of S could mean either the incorrect information of the boundary does not affect

the estimated S or differences in S values are too small, although they are displayed as the low S zones in the contour plot (Figure 3). These characteristics of S are also shown in Figure 9, where the estimated S does not apparently scatter lower than 1:1 line as found in the estimated T. Compared to the estimated S in Case 1 (Figure 9a), the results of Case 2 and 3 (Figures 9b and 9c) are lined on a similar trend.

3. Role of prior information

Performance metricses are employed to evaluate the effects of prior information on the estimation. In this investigation, the simulations of ten realizations are considered. The plot of average and standard deviation in Table 1 and Figure 10 indicate that prior knowledge of basin boundary geometries and its conditions are the most important for estimating T and S. Inverse simulations with SimSLE in Case 1 always result in the highest R^2 and lowest L_1 and L_2 among these three cases. For the case using incorrect boundary geometries and conditions, the zonation based on geology knowledge in Case 3 can improve the estimation of T and S. The average of R^2, L_1, and L_2 of Case 3 slightly better than the performance metricses in Case 2, which using only one initial guess of T to represent both permeable and impermeable materials.

Moreover, the prior information in each condition A, B, and C are also examined. Although the simulation of T with condition A (steady-state) does not account for an effect of S in the estimation, L_1 and L_2 of T in this condition are larger than the other conditions due to fewer data points of drawdown. These results of the estimates between steady and transient state simulations are consistent with the study by Liu et al. (2007). In condition B, information about the true distribution of S was used. It turns out that this true S can improve the estimated T only for Case 1, in which the assigned boundary geometries and conditions are correct. On the other hand, with the incorrect boundary in Case 2 and Case 3, this true S distribution does not play an important

role in the estimation. The performance metricses do not show any improvement in Case 2B and Case 3B. For condition C (uniform initial guess of S), the results of Case 1 are moderately worse than using the true S (condition B). On the contrary, condition C slightly improves the estimated T of incorrect boundary cases (Case 2 and 3). L_1 and L_2 of Case 2C and 3C are smaller than in Case 2B and 3B.

Lastly, the estimated S in condition C, which is started with the uniform initial guess of S, is considered. Average R^2 of many realizations of Case 1 (Table 2) is not obviously different from Case 2 and Case 3 compared to the differences in average R^2 in the estimated T cases. Due to the very small S values, L_1 and L_2 of estimated S in each condition are in the same magnitude.

CONCLUSIONS

With incorrect guess constant head boundary conditions, HT identifies the true impermeable boundaries as lower T zones along the boundary. These estimated low T zones generally outline the irregular shape of the impermeable boundary of the aquifer. Estimated S shows these characteristics of low S zones as well; but, due to the small number of S, the estimated low S zones do not show apparent deviation from the true values compared to the estimated low T zones.

The comparison of the estimates inside the basin in every case leads to the conclusion that boundary conditions are significant to parameter estimation. The case with correct boundary geometries and conditions (Case 1) always results in a better estimation of T and S.

The zonation of the initial guesses of T and S based on knowledge of geology improves the estimation compared to the case using only the mean properties of the aquifer. Using the true S field as the prior information improves the estimation only in the case that boundary geometries and conditions are correctly defined (Case 1). On the contrary, using the average value of S yields a better estimation in the cases with incorrect boundary geometries and conditions (Case 2 and Case 3).

While simulations with more realizations should be conducted in order to draw a definitive conclusion for the estimation, this study shows that the means of performance metricses from Monte Carlo simulation is necessary to evaluate the results of an inverse problem. This is an important contribution of this study to the inverse modeling of ill-defined problems.

APPENDIX A: TABLES

Table 1: Performance metrics of the estimated T from ten realizations.

Performance Metrics	Conditions	Case 1		Case 2		Case 3	
		Mean	SD	Mean	SD	Mean	SD
R^2	A	0.6724	0.0738	0.4573	0.0935	0.4868	0.1013
	B	0.7558	0.1021	0.4401	0.1091	0.4953	0.1036
	C	0.6942	0.0917	0.4973	0.1264	0.5512	0.1236
L_1	A	0.5644	0.0690	0.9073	0.1404	0.7814	0.1241
	B	0.4815	0.0945	0.7915	0.1021	0.7056	0.1135
	C	0.5680	0.0969	0.7400	0.1228	0.6644	0.1110
L_2	A	0.5449	0.1273	1.4589	0.3639	1.1183	0.2959
	B	0.3969	0.1689	1.3440	0.3067	1.0372	0.2144
	C	0.5606	0.1819	1.0422	0.2714	0.7866	0.2213
Slope	A	0.6693	0.1023	0.6930	0.1082	0.6623	0.1052
	B	0.7624	0.0958	0.7163	0.1179	0.7112	0.1034
	C	0.6858	0.1109	0.7019	0.1170	0.6540	0.1178
Intercept	A	-0.3929	0.1490	-0.9930	0.3891	-0.9055	0.2051
	B	-0.3257	0.1252	-0.7757	0.1705	-0.6691	0.1485
	C	-0.2309	0.1271	-0.7092	0.1526	-0.6259	0.1325

Table 2: Performance metrics of the estimated S from ten realizations.

Performance Metrics	Conditions	Case 1		Case 2		Case 3	
		Mean	SD	Mean	SD	Mean	SD
R^2	C	0.6530	0.1034	0.5918	0.1132	0.5980	0.1211
L_1	C	3.85E-04	6.40E-05	4.08E-04	7.10E-05	4.50E-04	1.69E-04
L_2	C	3.46E-07	1.14E-07	4.31E-07	1.66E-07	5.00E-07	2.96E-07
Slope	C	0.5359	0.1375	0.5363	0.1072	0.4516	0.3155
Intercept	C	-3.2604	0.9396	-3.3526	0.7508	-4.0003	2.3508

APPENDIX B: FIGURES

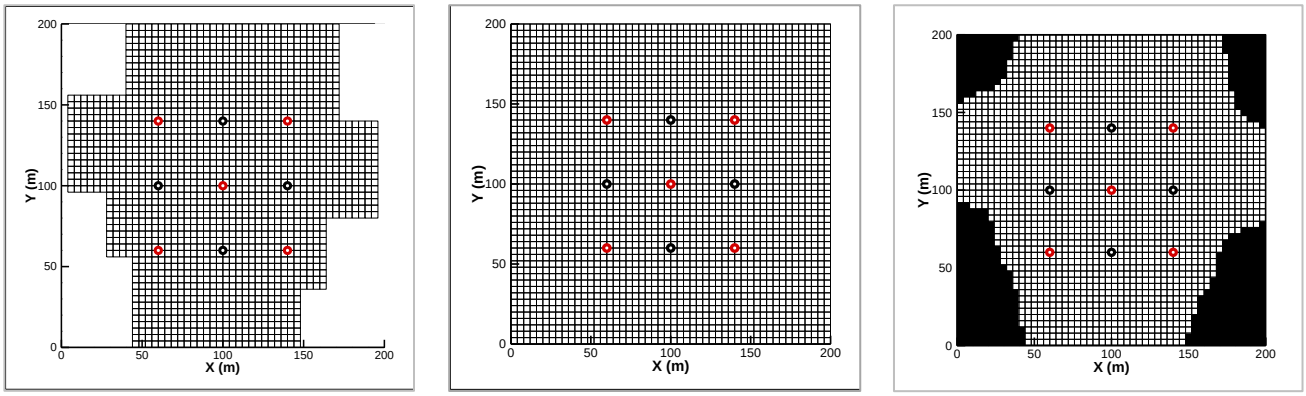

(a) (b) (c)

Figure 1. Model geometries of (a) a synthetic aquifer and Case 1, (b) Case 2, and (c) Case 3

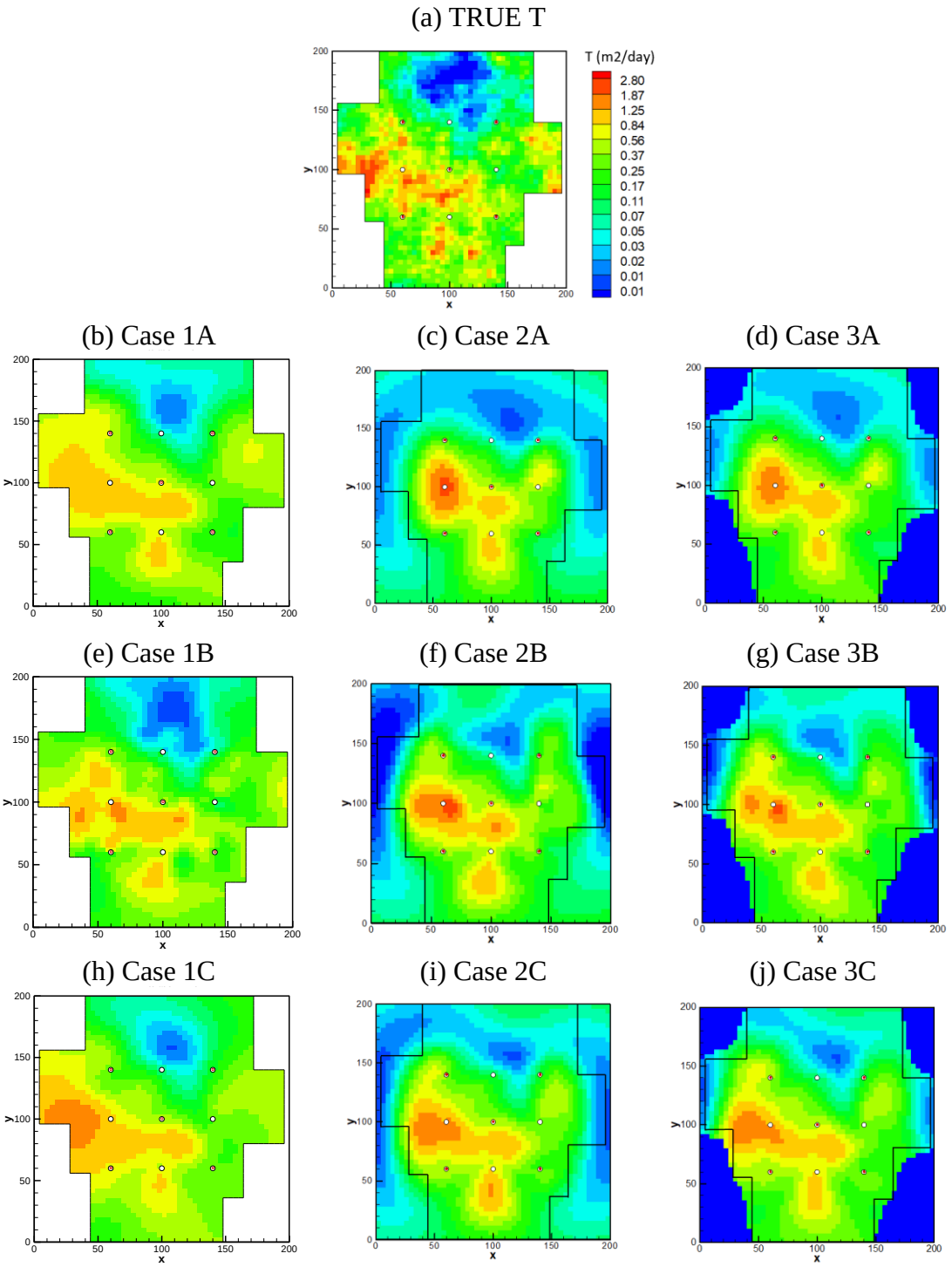

Figure 2. Contour plots of (a) the true synthetic T field compared to the estimated T of (b, e, h) Case1, (c, f, i) Case 2, and (d, g, j) Case 3. A, B, and C notation indicate the simulation in a steady-state, a transient state with true S information, and a transient state with uniform S, respectively. Every plot is in the same color scale.

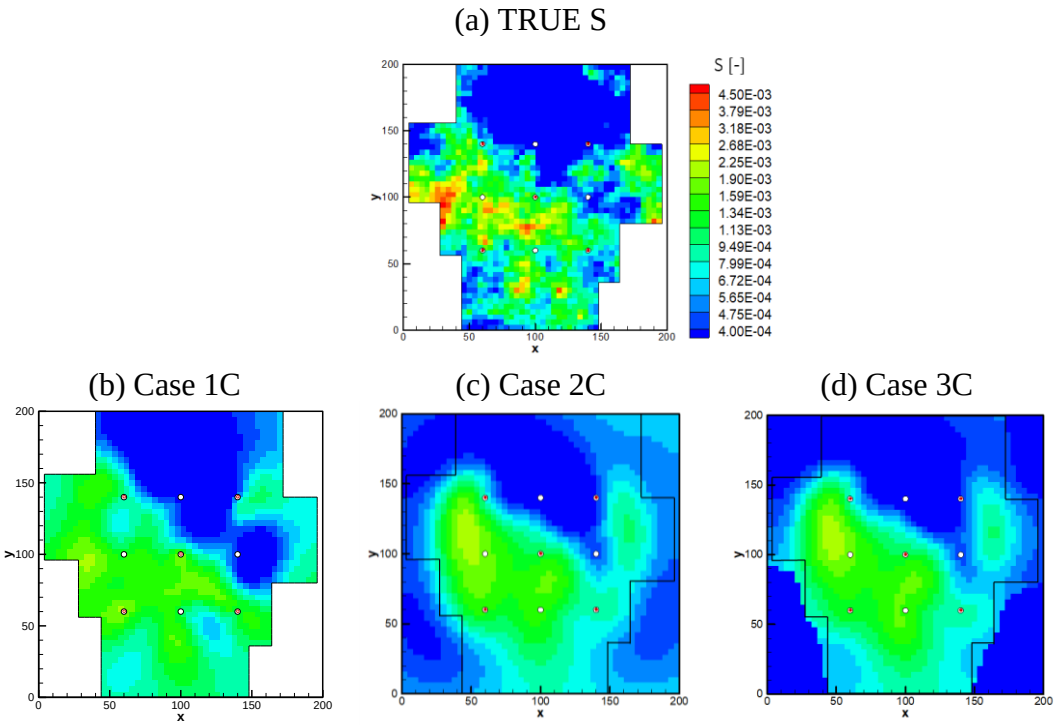

Figure 3. Contour plots of (a) the true distribution of synthetic S compared to the estimated S of (b) Case 1C, (c) Case 2C, and (d) Case 3C. Every plot is in the same color scale.

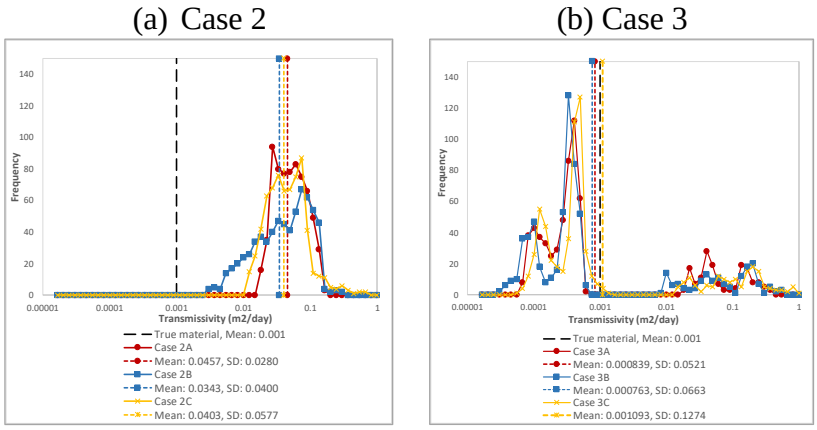

Figure 4. Distribution of the estimated T at elements outside the basin area of (a) Case 2 and (b) Case 3.

(a) Case 2C (b) Case 3C

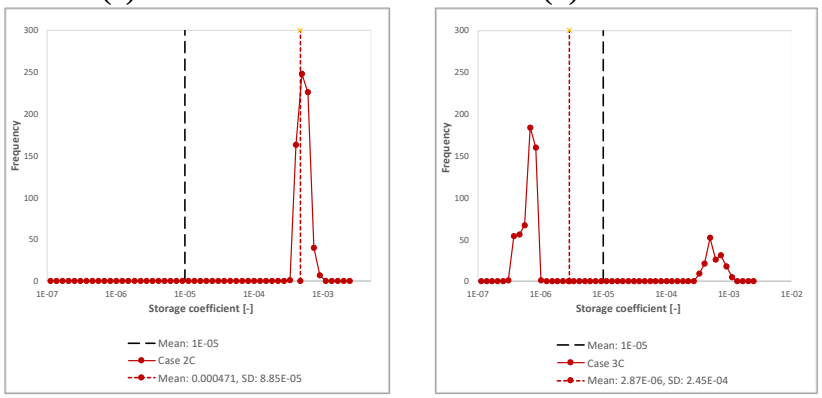

Figure 5. Distribution of the estimated S at elements outside the basin area of (a) Case 2C and (b) Case 3C.

(a) Case 1 (b) Case 2 (c) Case 3

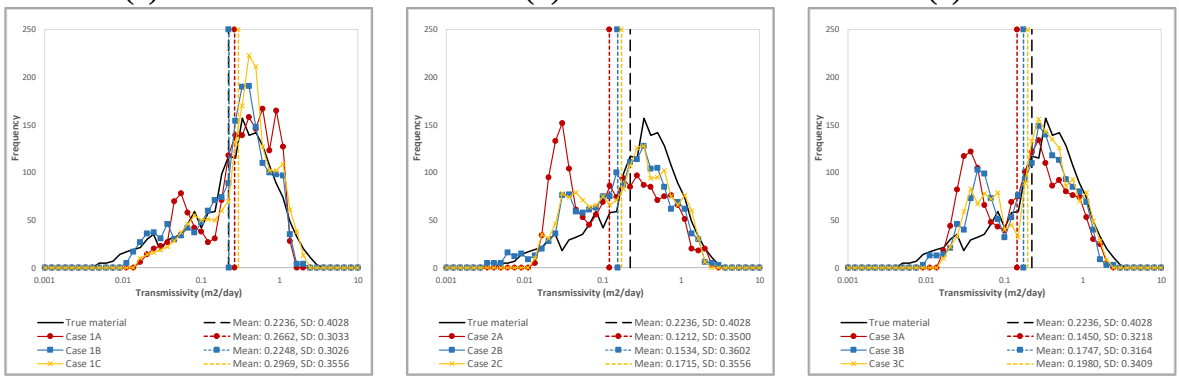

Figure 6. Distribution of the estimated T in the basin area of (a) Case 1, (b) Case 2, and (c) Case 3.

(a) Case 1C (b) Case 2C (c) Case 3C

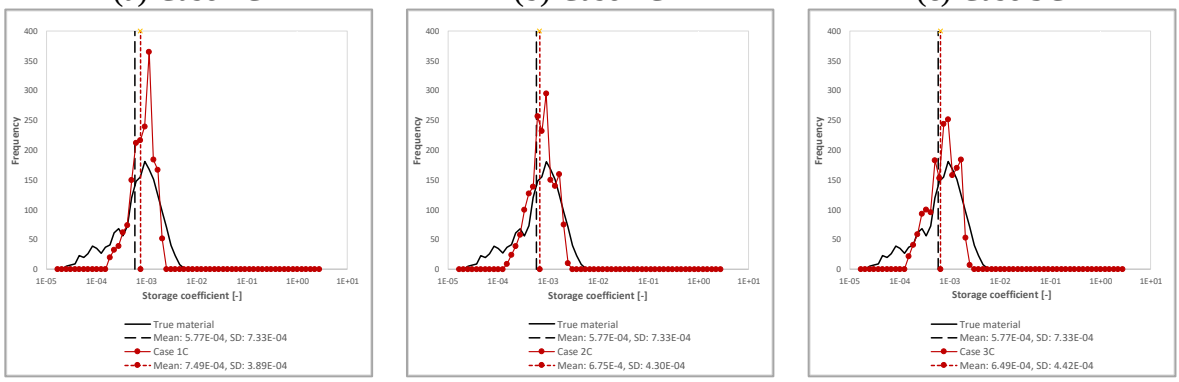

Figure 7. Distribution of the estimated S in the basin area of (a) Case 1C, (b) Case 2C, and (c) Case 3C.

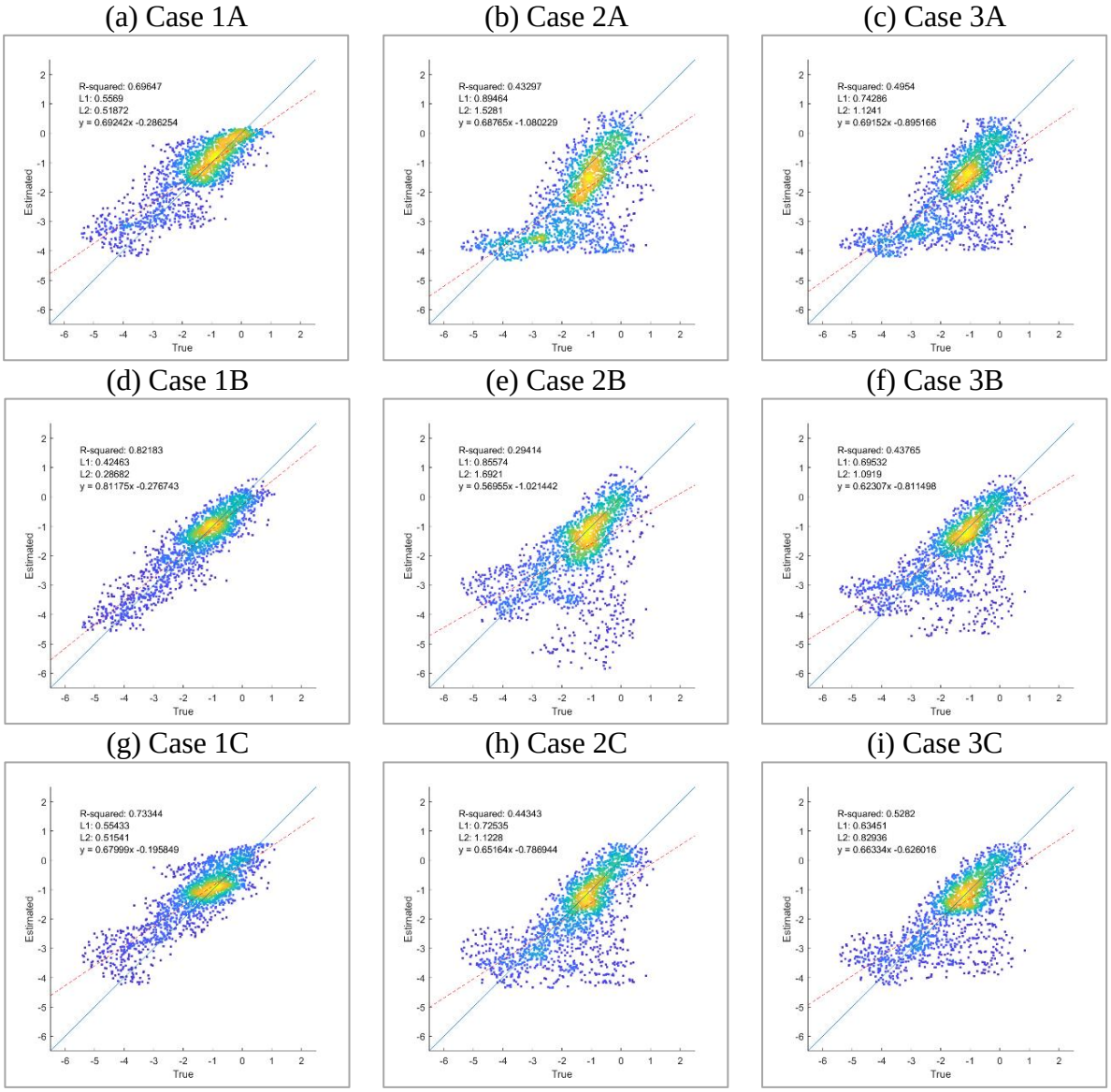

Figure 8. Scatter plots of true versus estimated T of (a, d, g) Case 1A, 1B, 1C, (b, e, h) Case 2A, 2B, 2C, and (c, f, i) Case 3A, 3B, 3C in log scale.

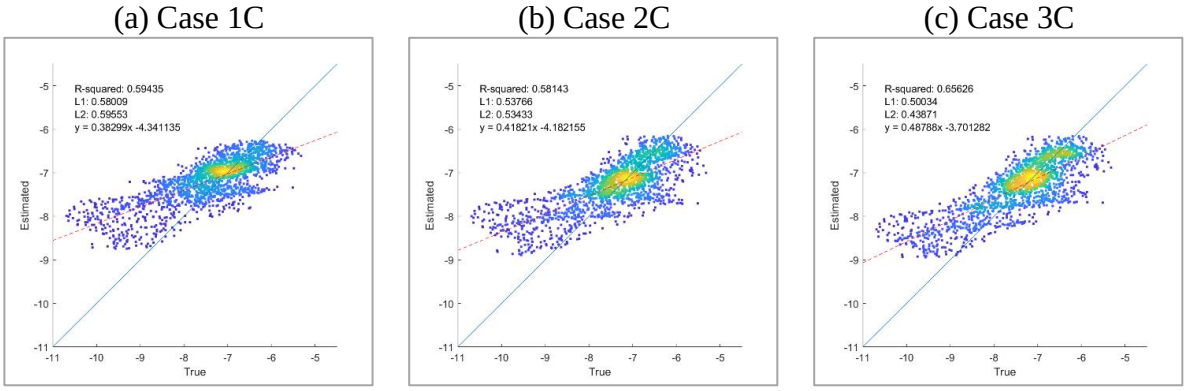

Figure 9. Scatter plots of true versus estimated S of (a) Case 1C, (b) Case 2C, and (c) Case 3C in log scale.

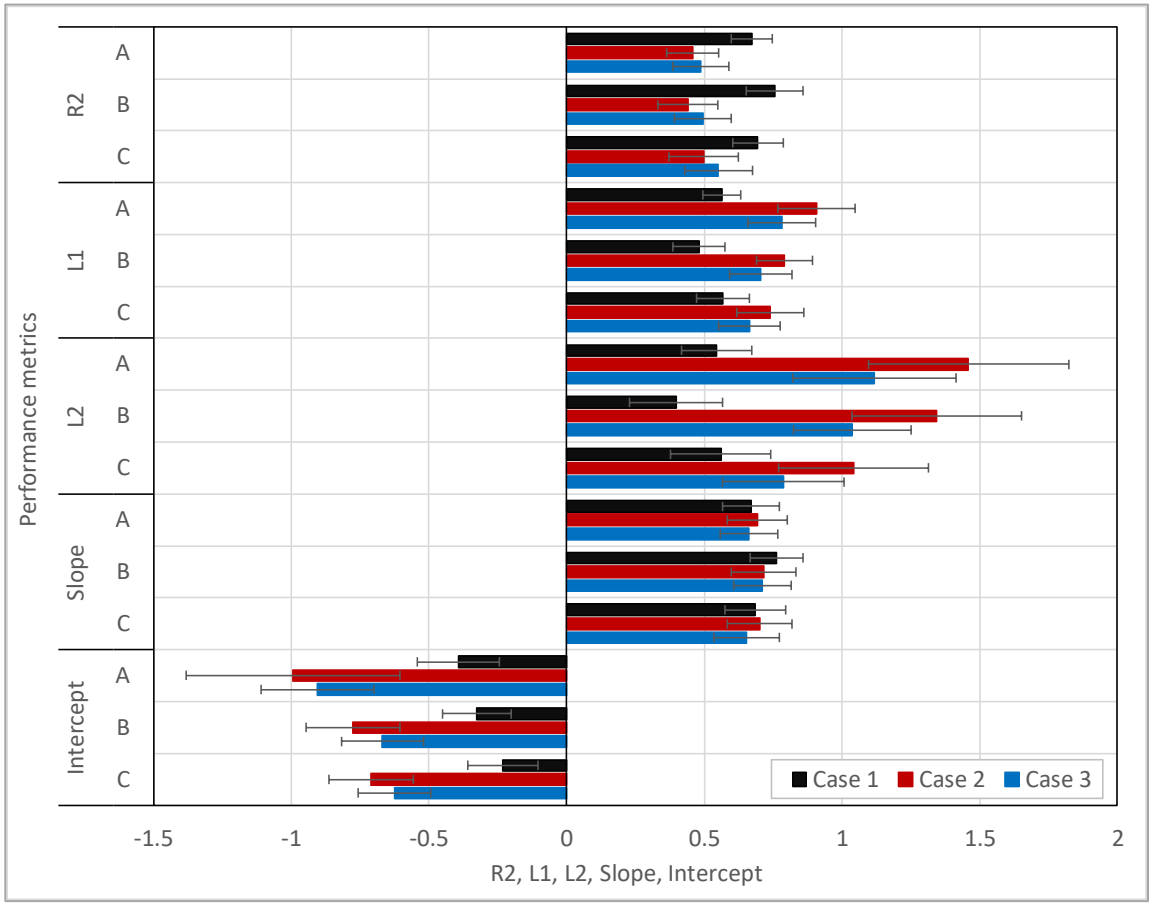

Figure 10. The calculated mean and standard deviation of performance metricses of each case over ten realizations.

REFERENCES

Anderson, M. P. (1989). Hydrogeologic facies models to delineate large-scale spatial trends in glacial and glaciofluvial sediments. Geological Society of America Bulletin, 101(4), 501–511. doi: 10.1130/0016-7606(1989)101

Berg, S. and Illman, W. (2012). Field Study of Subsurface Heterogeneity with Steady-State Hydraulic Tomography. *Ground Water*, 51(1), pp.29-40.

Bohling, G. and Butler, J. (2010). Inherent Limitations of Hydraulic Tomography. Ground Water, 48(6), pp.809-824.

Cardiff, M., Barrash, W. and Kitanidis, P. (2012). A field proof-of-concept of aquifer imaging using 3-D transient hydraulic tomography with modular, temporarily-emplaced equipment. Water Resources Research, 48(5).

Cardiff, M. and Barrash, W. (2011). 3-D transient hydraulic tomography in unconfined aquifers with fast drainage response. Water Resources Research, 47(12).

Cooper, H. and Jacob, C. (1946). A generalized graphical method for evaluating formation constants and summarizing well-field history. *Transactions, American Geophysical Union*, 27(4), p.526.

Huang, S.-Y., Wen, J.-C., Yeh, T.-C. J., Lu, W., Juan, H.-L., Tseng, C.-M., Lee, J.-H., Chang, K.-C. (2011). Robustness of joint interpretation of sequential pumping tests: Numerical and field experiments. Water Resources Research, 47(10). doi: 10.1029/2011wr010698

Illman, W., Berg, S. and Zhao, Z. (2015). Should hydraulic tomography data be interpreted using geostatistical inverse modeling? A laboratory sandbox investigation. Water Resources Research, 51(5), pp.3219-3237.

Liu, S., Yeh, T. and Gardiner, R. (2002). Effectiveness of hydraulic tomography: Sandbox experiments. *Water Resources Research*, 38(4), pp.5-1-5-9.

Liu, X., Illman, W., Craig, A., Zhu, J. and Yeh, T. (2007). Laboratory sandbox validation of transient Liu, X., Illman, W. A., Craig, A. J., Zhu, J., & Yeh, T.-C. J. (2007).

Mao, D., T.-C. J. Yeh, L. Wan, C.-H. Lee, K.-C. Hsu, J.-C. Wen, and W. Lu (2013), Cross-correlation analysis and information content of observed heads during pumping in unconfined aquifers, Water Resour. Res., 49, 713–731, doi:10.1002/wrcr.20066.

Ni, C., Yeh, T. and Chen, J. (2009). Cost-Effective Hydraulic Tomography Surveys for Predicting Flow and Transport in Heterogeneous Aquifers. *Environmental Science & Technology*, 43(10), pp.3720-3727.

Straface, S., Yeh, T., Zhu, J., Troisi, S. and Lee, C. (2007). Sequential aquifer tests at a well field, Montalto Uffugo Scalo, Italy. *Water Resources Research*, 43(7).

Theis, C. (1935). The relation between the lowering of the Piezometric surface and the rate and duration of discharge of a well using ground-water storage. *Transactions, American Geophysical Union*, 16(2), p.519.

Tso, M. C., Zha, Y., Yeh, T. and Wen, J. (2016). The relative importance of head, flux, and prior information in hydraulic tomography analysis. *Water Resources Research*, 52(1), pp.3-20.

Wen, J., Chen, J., Yeh, T., Wang, Y., Huang, S., Tian, Z. and Yu, C. (2019). Redundant and Nonredundant Information for Model Calibration or Hydraulic Tomography. Groundwater.

Wen, J., Wu, C., Yeh, T. and Tseng, C. (2010). Estimation of effective aquifer hydraulic properties from an aquifer test with multi-well observations (Taiwan). *Hydrogeology Journal*, 18(5), pp.1143-1155.

Xiang, J., Yeh, T. J., Lee, C., Hsu, K., & Wen, J. (2009). A simultaneous successive linear estimator and a guide for hydraulic tomography analysis. *Water Resources Research*,*45*(2). doi:10.1029/2008wr007180

Yeh, T., Khaleel, R., Carroll, K.C. (2015**).** Flow Through Heterogeneous Geological Media, *Cambridge University Press*, Cambridge

Yeh, T. and Lee, C. (2007). Time to Change the Way We Collect and Analyze Data for Aquifer Characterization. Ground Water, 45(2), pp.116-118.

Yeh, T. and Liu, S. (2000). Hydraulic tomography: Development of a new aquifer test method. *Water Resources Research*, 36(8), pp.2095-2105.

Yeh, T., Srivastava, R., Guzman, A., Harter, T. (1993). A Numerical Model for Water Flow and Chemical Transport in Variably Saturated Porous Media. *Ground Water*, 31(4), pp.634-644.

Yeh, T. (1992). Stochastic modeling of groundwater flow and solute transport in aquifers. *Hydrological Processes*, 6(4), pp.369-395.

Yin, D. and Illman, W. (2009). Hydraulic tomography using temporal moments of drawdown recovery data: A laboratory sandbox study. *Water Resources Research*, 45(1).

Zha, Y., Yeh, T., Illman, W., Onoe, H., Mok, C., Wen, J., Huang, S. and Wang, W. (2017). Incorporating geologic information into hydraulic tomography: A general framework based on geostatistical approach. *Water Resources Research*, 53(4), pp.2850-2876.

Zha, Y., Yeh, T., Illman, W., Tanaka, T., Bruines, P., Onoe, H., Saegusa, H., Mao, D., Takeuchi, S. and Wen, J. (2016). An Application of Hydraulic Tomography to a Large-scale Fractured Granite Site, Mizunami, Japan. *Groundwater*, 54(6), pp.793-804.

Zhu, J. and Yeh, T. (2005). Characterization of aquifer heterogeneity using transient hydraulic tomography. Water Resources Research, 41(7).